Eliminate Reactive Power and Increase System Efficiency of Isolated Bidirectional Dual-Active-Bridge DC–DC Converters Using Novel Dual-Phase-Shift Control

Hua Bai and Chris Mi, *Senior Member, IEEE*

***Abstract*—This paper proposes a novel dual-phase-shift (DPS) control strategy for a dual-active-bridge isolated bidirectional dc–dc converter. The proposed DPS control consists of a phase shift between the primary and secondary voltages of the isolation transformer, and a phase shift between the gate signals of the diagonal switches of each H-bridge. Simulation on a 600-V/5-kW prototype shows that the DPS control has excellent dynamic and static performance compared to the traditional phase-shift control (single phase shift). In this paper, the concept of "reactive power" is defined, and the corresponding equations are derived for isolated bidirectional dc–dc converters. It is shown that the reactive power in traditional phase-shift control is inherent, and is the main factor contributing to large peak current and large system loss. The DPS control can eliminate reactive power in isolated bidirectional dc–dc converters. In addition, the DPS control can decrease the peak inrush current and steady-state current, improve system efficiency, increase system power capability (by 33%), and minimize the output capacitance as compared to the traditional phase-shift control. The soft-switching range and the influence of short-time-scale factors, such as deadband and system-level safe operation area, are also discussed in detail. Under certain operation conditions, deadband compensation can be implemented easily in the DPS control without a current sensor.**

***Index Terms*—DC–DC converter, deadband, dual active bridge (DAB), phase-shift control, reactive power, safe operational area (SOA).**

I. Introduction

POWER electronic converters are used extensively in personal electronics, power systems, hybrid electric vehicles (HEVs), and many other applications to provide dc voltage sources and manage power flow by switching actions [1], [2]. To obtain high power quality, switching control strategies that can achieve high performances are attracting more and more attention [3], [4]. Many advanced control strategies, such as fuzzy-neural control or sliding-mode control [3], [4], have been proposed to enhance the steady-state and dynamic performance of power electronic systems. Although these control strategies are predicted to be promising in more complex-structured converters, such as dual-active-bridge (DAB) dc–dc converters [5], most of the present applications are still confined to simple-structured circuits, such as buck, boost, and half-bridge converters [6], [7].

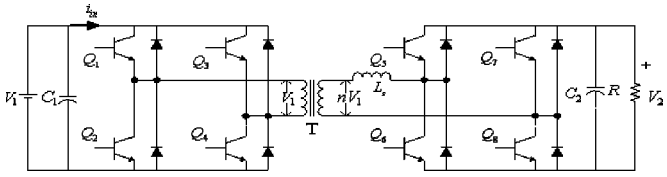

Fig. 1. Electrical systems in a series HEV.

Compared to traditional dc–dc converter circuits, isolated bidirectional DAB dc–dc converters illustrated in Fig. 1 have many advantages, such as electrical isolation, high reliability, ease of realizing soft-switching control, and bidirectional energy flow [8], [9]. The control algorithm for such topology is mainly limited to a PI-based phase-shift control [1], [9]. In this traditional phase-shift control, the gate signals of the diagonal semiconductors, e.g., (Q_1, Q_4) in Fig. 1, are the same. The gate signals of the corresponding switches in the primary and the secondary bridges are phase-shifted. This control algorithm is simple and easy to implement, but it is essentially an active-power-centered control algorithm. It not only lacks flexibility but also brings additional stress to the devices used in the system during steady-state operation and the starting-up process. In order to improve the system performance, various control algorithms were explored. A phase-shift plus pulsewidth modulation (PWM) and zero-voltage switching (ZVS)–PWM control are presented in [10] and [11], respectively. In these studies, the duty ratio of the gate signals of each semiconductor device is variable, and should be calculated online.

A double-phase-shift control for a unidirectional three-level converter is proposed in [12]. The phase shift is implemented on the primary side. A start-up circuit to suppress the inrush current with a set of auxiliary circuits is proposed in [13]. Until this point, there is no mature control or topology to depress the inrush current in the starting process of isolated dc–dc converters.

It needs to be pointed out that, in the proposed dual-phase-shift (DPS) control, when C_1 is charged, there is still a big inrush current. The inrush current should be controlled by the peripheral circuitry that is beyond the scope of our paper.

This paper proposes a novel concept, DPS control, which adds another degree of freedom to the system by adjusting the

Manuscript received March 13, 2008; revised July 14, 2008. Current version published December 9, 2008. Recommended for publication by Associate Editor P. Jain.

The authors are with the Department of Electrical and Computer Engineering, University of Michigan, Dearborn, MI 48128 USA (e-mail: chrismi@umich.edu).

Color versions of one or more of the figures in this paper are available online at http://ieeexplore.ieee.org.

Digital Object Identifier 10.1109/TPEL.2008.2005103

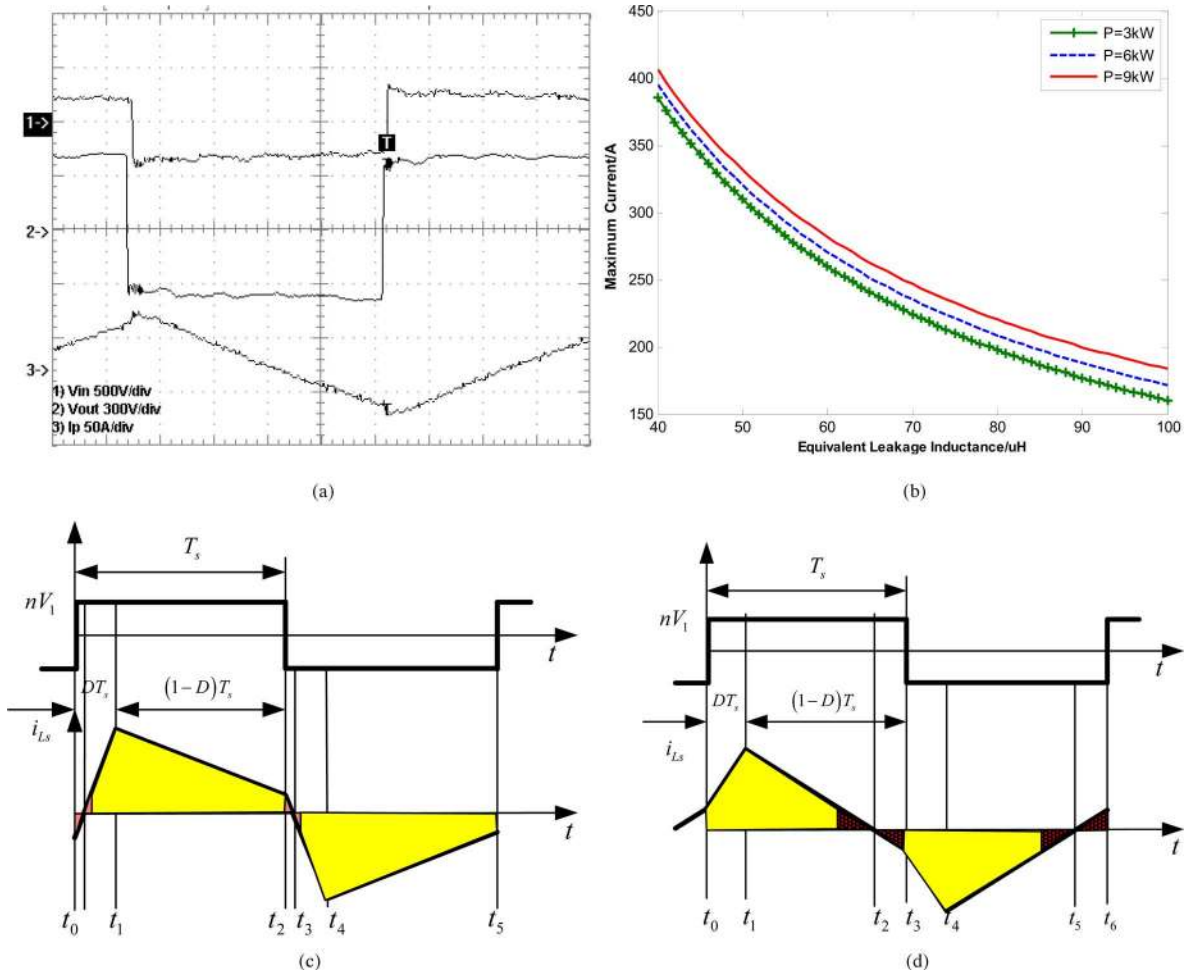

Fig. 2. Current waveforms under different operational states. (a) $V_1 = 205$ V, $V_2 = 270$ V. (b) Maximum current under different load. (c) Heavy-load condition. (d) Light-load condition.

time sequence between the gate signals of diagonal semiconductor switches, e.g., (Q_1, Q_4) in Fig. 1. Theoretical analysis shows that the proposed control strategy provides better dynamic and static performance than the traditional phase-shift control. The proposed DPS control can decrease peak current, eliminate reactive power, increase power capability, increase system efficiency, and minimize the output capacitance. The DPS control can also be used in the starting process to limit the inrush current. This is particularly useful in high-voltage and high-power converters where the safe operation area (SOA) is difficult to design. The influence of some short-time-scale physical parameters on the control algorithm, such as deadband and its compensation, are discussed in detail.

II. Reactive Power in DAB DC–DC Converters

In Fig. 1, if we assume energy flows from the primary (V_1) to the secondary (V_2) and neglect losses, then the power of the system for traditional phase-shift control is [14]

$$P = \frac{nV_1V_2D(1-D)}{2f_sL_s} \tag{1}$$

where D is the phase-shift ratio between the primary and secondary voltages of the isolation transformer, n is the turns ratio of the transformer, V_1 is the transformer primary voltage, L_s is the equivalent leakage inductance of the transformer, and V_2 is the output voltage, and C_1 and C_2 are the primary and secondary dc-link capacitors, respectively.

In traditional phase-shift-based DAB dc–dc converters, only a phase shift D between the primary and secondary voltages of the transformer is involved. In Fig. 1, the gate signals of Q_1 and Q_4 (or Q_2 and Q_3) are always at 50% duty ratio with a square-waveform output at the primary of the transformer. The gate signals of Q_1 and Q_5 (or Q_3 and Q_7) are shifted in phase. Such control is simple and easy to implement. Since there is only one phase shift used in this control, this is named single-phase-shift (SPS) control.

With SPS control, the maximum current $I_{\max}$ and initial current I_o in the transformer of the DAB converter in each of the switching periods during steady-state operation can be expressed as

$$I_{\max} = \frac{n}{4f_SL_S}[-(1-2D)nV_1 + V_2] \tag{2}$$

$$I_0 = \frac{n}{4f_SL_S}[(1-2D)V_2 - nV_1]. \tag{3}$$

Fig. 2(a) shows the measured current and voltage waveforms of a prototype DAB dc–dc converter with SPS control

for $V_1 = 205$ V, $V_2 = 270$ V, and $P_o = 0$. It can be seen from (2), (3), and Fig. 2 that when $V_2 \neq nV_1$, there is always a current flowing in the transformer, even for phase shift $D = 0$ (where output power $P = 0$). When $V_2 = nV_1$, there is always a current flowing in the transformer, except for $D = 0$. This current contributes to the reactive power in the circuit.

Fig. 2(b) shows the peak current in steady-state operation as a function of leakage inductance and output power. It can be seen that for a given leakage inductance, the current does not change very much as the output power changes. A considerable portion of the current is contributing to the reactive power, especially under light-load conditions. The large current at low-power output operations results in lower system efficiency and large electrical stress on the semiconductor switches.

For traditional buck, boost, or half-bridge converters, there is no reactive power since all the power flows from the power supply to the load or feeds back from the load to the power source within one switching cycle. For bidirectional DAB converters, the primary and secondary voltages applied to the transformer are both square-wave ac. Their interaction is through the leakage inductance of the transformer. Therefore, the phase of the primary current is not always the same as the primary voltage. A portion of the power delivered to the load in one switching period is consumed by the load resistor, while the other portion is sent back to the primary voltage source. This is defined as reactive power in isolated bidirectional dc–dc converters. Fig. 2(c) and (d) illustrates the phase difference between the voltage and current of the transformer secondary caused by phase shift. The reactive power, which is the dark shaded area in Fig. 2(c) and (d), is defined as

$$Q = \frac{1}{T_s} nV_1 \int_{t_2}^{t_3} i(t)\, dt. \tag{4}$$

The polarity of transformer primary voltage will change at $t = t_3$. In Fig. 2(c), $i(t_2) > 0$ and $i(t_3) = 0$. In Fig. 2(d), $i(t_2) = 0$ and $i(t_3) < 0$. Assuming $nV_1 < V_2$ and substituting (3) in (4), the expression of reactive power can be derived as

$$Q = nV_1 \frac{[(1-2D)V_2 - nV_1]^2}{16 f_S L_S} \times \begin{cases} \dfrac{1}{nV_1 + V_2}, & I_0 < 0 \\ 0, & I_0 = 0 \\ \dfrac{1}{nV_1 - V_2}, & I_0 > 0. \end{cases} \tag{5}$$

A positive Q corresponds to heavy-load operation conditions, where $I_0 < 0$, and the current is lagging the voltage. Therefore, positive Q is the inductive reactive power. A negative Q corresponds to light-load operation conditions, where $I_0 > 0$, and the current is leading the voltage. Therefore, a negative Q is the capacitive reactive power.

It can be seen from (5) that except for the operational mode where $(1-2D)V_2 = nV_1$, there is always reactive power flowing in the system. This portion of power does not contribute to the output power, but increases the system loss and brings high current impact on the semiconductor switches. Light-load operations are accompanied by large reactive power.

III. DPS Control of DAB DC–DC Converters

A method to balance the reactive and active powers in parallel connected inverters is proposed in [15]. In the proposed DPS control, the goal is not only to "control" the reactive power, but also to eliminate it totally. In order to significantly decrease the current, and thus, reactive power of the DAB system, V_1 or V_2 should not be confined to square waveforms with 50% duty ratio. For example, if Q_1 and Q_4 do not have the same gate signal, but have a phase shift of D_1, as shown in Fig. 3(a), the transformer primary and secondary voltages will emerge as a three-level instead of the traditional two-level. The duty ratio is $\mu = 1 - D_1$. The phase shift between the transformer primary and secondary voltages is now defined as D_2. From Fig. 3(a), when $D_1 \leq 1/2$, the expression of the output power is

$$P = \frac{nV_1V_2}{2f_sL_S} \times \begin{cases} D_2(2-2D_1-D_2), & 0 \leq D_2 \leq D_1 \\ D_2(1-D_1-D_2)+D_1-D_1^2, & D_1 \leq D_2 \leq 1-D_1 \\ (1-D_1)(1-D_2), & 1-D_1 \leq D_2 \leq 1 \end{cases} \tag{6}$$

when $D_1 > 1/2$

$$P = \frac{nV_1V_2}{2f_sL_S} \times \begin{cases} D_2(2-2D_1-D_2), & 0 \leq D_2 \leq 1-D_1 \\ (1-D_1)^2, & 1-D_1 \leq D_2 \leq D_1 \\ (1-D_1)(1-D_2), & D_1 \leq D_2 \leq 1. \end{cases} \tag{7}$$

The traditional SPS control has only one phase shift (D) that is between V_1 and V_2. The proposed DPS control presented in Fig. 3(a) has two phase shifts. The contour lines in Fig. 3(b) show that there are infinite combinations of (D_1, D_2) for the same output power P. The global maximum power is at $(D_1 = 1/3, D_2 = 1/3)$ via the partial derivatives of (6) and (7). The maximum output power is 4/3 times of the SPS control. Hence, the DPS control offers larger power output capability than does the SPS control.

The calculation of reactive power in the DPS system is rather complex. For illustration purposes, only one operation condition is considered, where $nV_1 = V_2$ and $D_1 \leq 1/2$. The expression of reactive power is shown in (8). At operation conditions where $D_2 < 1/2$, the reactive power is always zero

$$Q = \frac{nV_1V_2}{2f_sL_S} \times \begin{cases} 0, & 0 < D_2 < D_1 \\ 0, & D_1 < D_2 < 1-D_1 \\ \dfrac{(nV_1)^2}{16L_Sf_S}(D_1-D_2)^2, & 1-D_1 < D_2 < 1. \end{cases} \tag{8}$$

In the simulation of this paper, D_1 and D_2 are tuned by two separate PI modulators. When less output power is required, D_1 will increase while D_2 will decrease to deliver less power. Fig. 4(a) shows the transformer primary voltage in the dynamic process. When V_1 collapses to a lower value, in order to maintain the same amount of output power, D_2 should be increased. Fig. 4(b) shows the dynamic performance of the two control algorithms under disturbance when the load resistance is changed

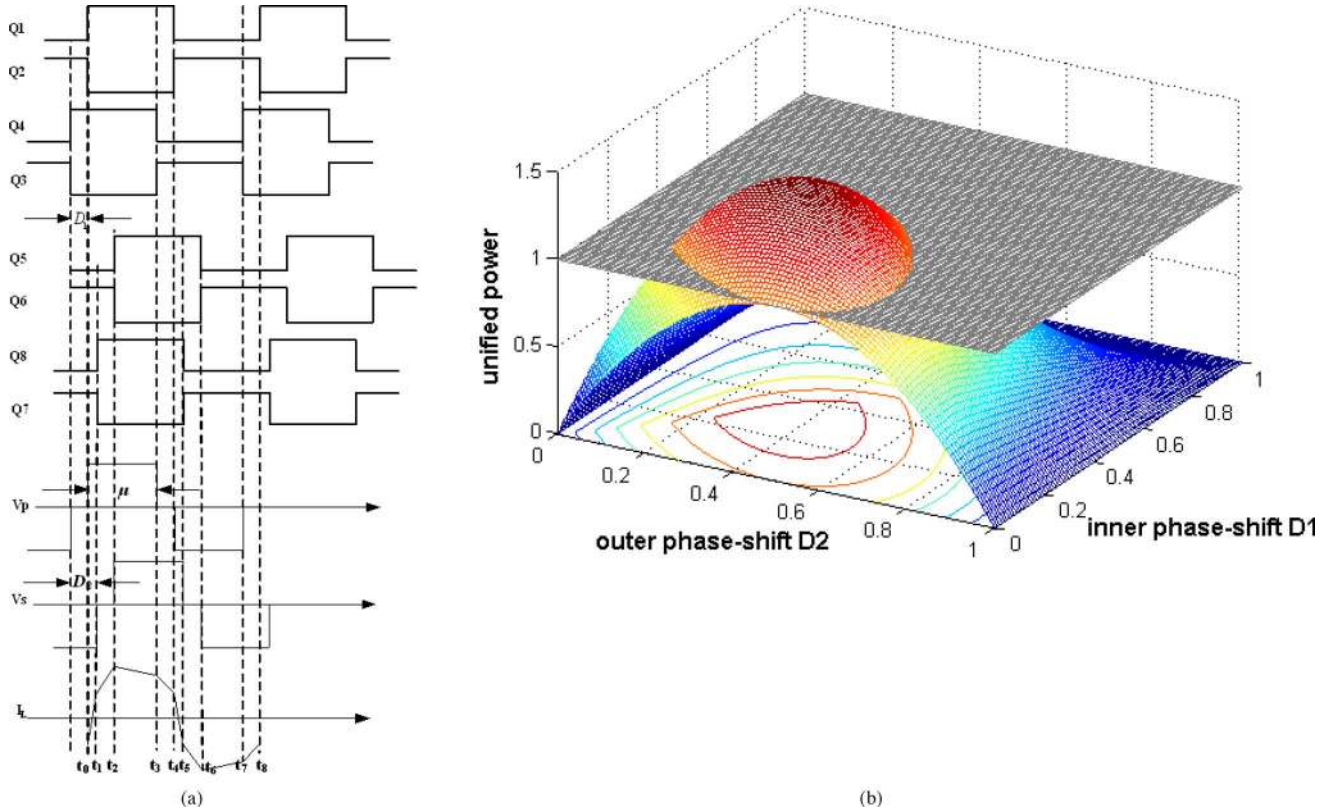

Fig. 3. Theory of DPS control. (a) Voltage waveforms of DPS. (b) Output power under different (D_1, D_2).

from 200 to 50 Ω at 30 ms. It can be seen from Fig. 4(b) that both static and dynamic performances of the DPS controlled system are much better than that of an SPS controlled system.

Fig. 4(c) shows the comparison of the transformer primary voltage for the two different control algorithms. Fig. 4(d) shows the transformer secondary currents for the two control algorithms. Under the same output power, the peak current of DPS control is much smaller than that of the SPS control. The reactive power is significantly erased from the system, while the active power remains the same. The elimination of reactive power results in a lower current and higher efficiency compared to the traditional SPS, especially under low-power output operations, as shown in Fig. 4(e). However, this calculation is based on the hard-switching mode. If soft-switching control is applied, this figure should be redrawn. The soft-switching range of DPS will be detailed in the following sections.

The peak currents for the two control algorithms are compared in Fig. 4(f). It can be seen that under low-power operation condition, the current of DPS control is less than that of the SPS control. This is helpful in reducing the system loss. It can also be seen from Fig. 4(f) that under the same equivalent leakage inductance, the DPS control can output more power than SPS control.

IV. Output Voltage Ripple

Another distinct advantage of the proposed DPS control is to reduce voltage ripple of the DAB dc–dc converter. Fig. 5 shows the output voltage ripple of the DAB system for the two control algorithms for $C_2 = 200\,\mu$F with the same PI parameters. DPS control has a significantly smaller output ripple than that of SPS control.

A smaller voltage ripple results from the smaller reactive power in the DAB system by DPS control. The secondary of the DAB system can be simplified, as shown in Fig. 6. In this equivalent circuit, when reactive power is delivered to the *RC* network, the voltage will be charged from $V_{\min}$ to $V_{\max}$

$$Q = \frac{1}{2}C(V_{\max}^2 - V_{\min}^2) = \frac{1}{2}C(V_{\max} - V_{\min})(V_{\max}+V_{\min}) = V_{\text{mean}}C\Delta V \tag{9}$$

and

$$\Delta V = \frac{Q}{V_{\text{mean}}C}. \tag{10}$$

Therefore, the output voltage ripple is directly proportional to the amount of reactive power in the circuit.

V. Implementation of DPS Control

Equation (7) shows that when $1 - D_1 \le D_2 \le D_1$, $P = nV_1V_2(1-D_1)^2/2f_sL_S$, the traditional phase shift D_2 is revoked, and the delivered power is determined only by the inner phase shift D_1. This could be named as an independent surface, as illustrated in Fig. 7.

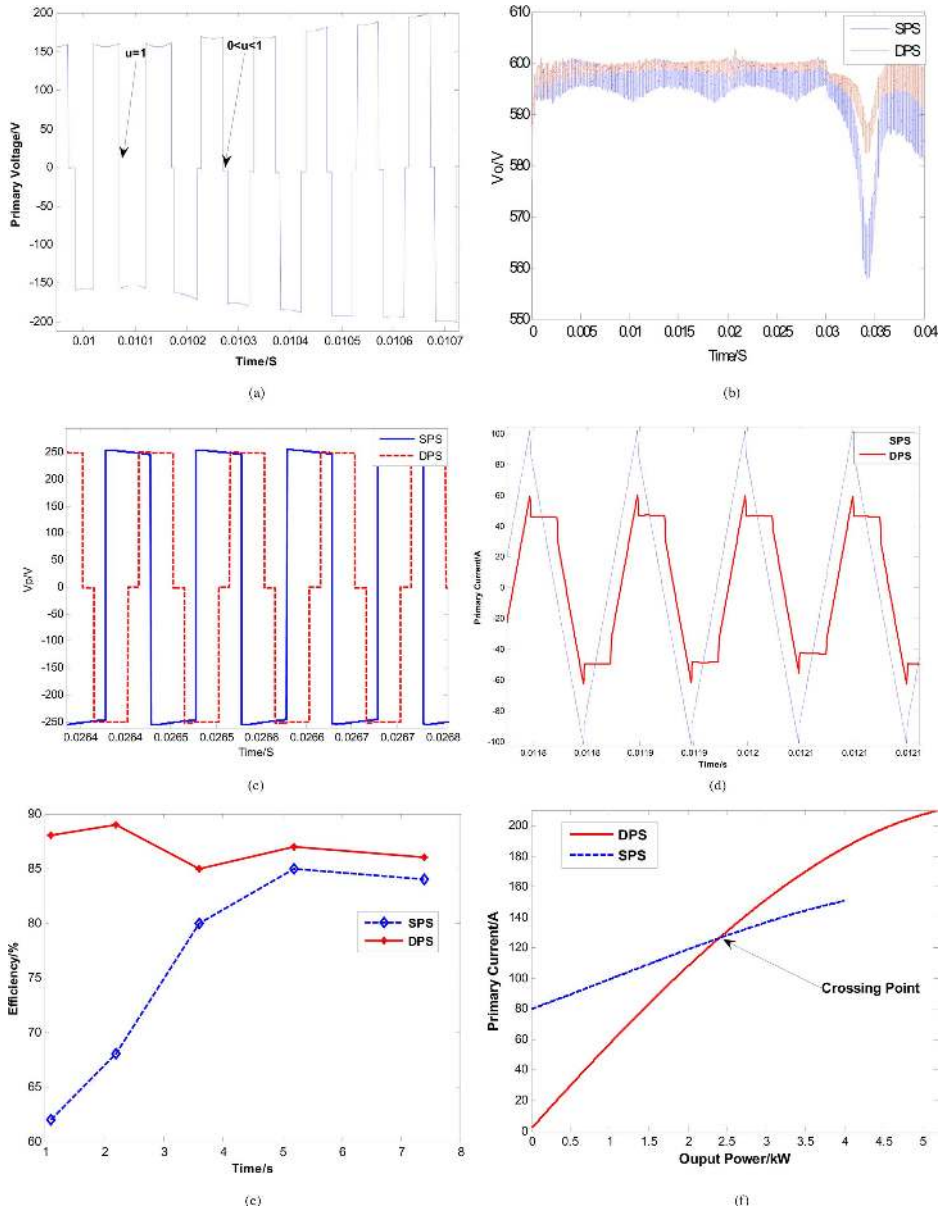

Fig. 4. Comparison of SPS and DPS. (a) Voltage waveforms of DPS. (b) Comparison of dynamic response of SPS and DPS. (c) Comparison of primary voltage of SPS and DPS. (d) Comparison of primary current of SPS and DPS. (e) Efficiency comparison of DPS and SPS. (f) Comparison of primary currents of DPS and SPS.

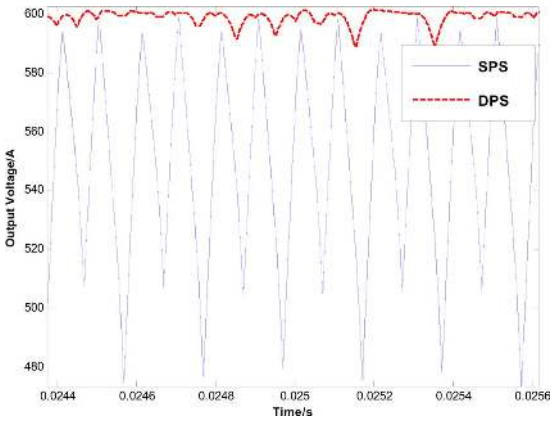

Fig. 5. Voltage ripple for the two control algorithms ($C = 200\,\mu$F).

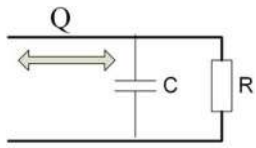

Fig. 6. Equivalent circuit of the output circuit of the DAB system.

Two PI modulators to tune (D_1, D_2) in real applications may not be practical. One of the methods to select (D_1, D_2) is to use the *independent surface*. Under the condition $1 - D_1 < D_2 < D_1$, the output power is determined only by the pulsewidth of the bridge output voltage, i.e., $1 - D_1$. In this case, D_2 can be set to 1/2, and only D_1 needs to be tuned with pulsewidth μ for the primary- and secondary-side voltages. When $nV_1 \leq V_2$,

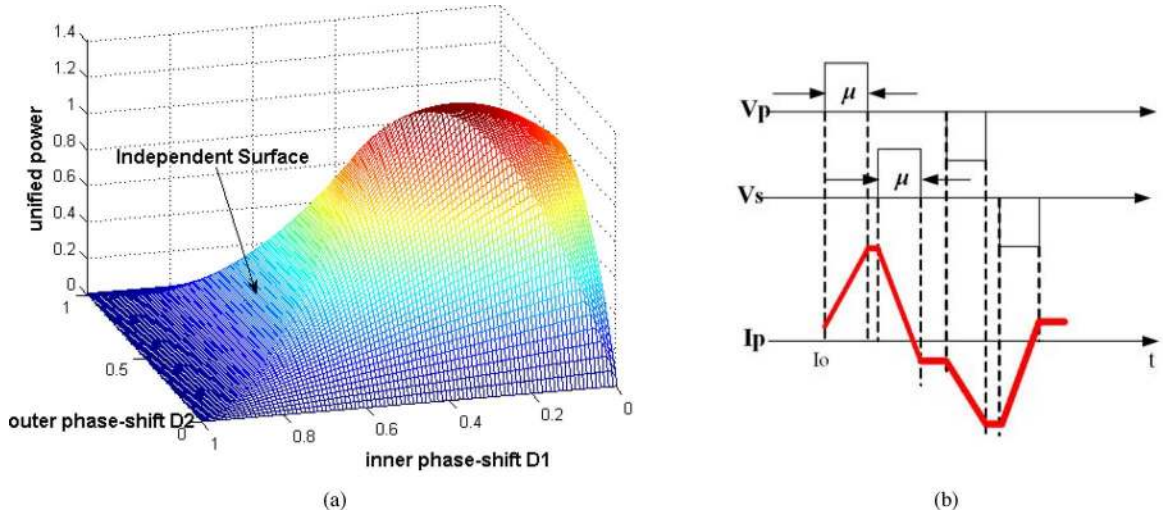

Fig. 7. Independent surface in the DPS control. (a) Independent surface. (b) Optimized sequence decreasing the reactive power where $nV_1 \leq V_2$.

initial current $I_0 \geq 0$. If and only if $nV_1 = V_2$, then $I_0 = 0$. At these circumstances, the reactive power is zero at all times, which could be analyzed from the time sequence of Fig. 7(b).

VI. Performance of SPS-Based Hard and Soft Starting of DAB DC–DC Converters

The start-up issue must be addressed in dc–dc converters, especially for high-voltage and high-power converters [13]. Fig. 8(a) and (b) corresponds to the condition where the initial voltage is 400 V, while the reference voltage is 600 V. Fig. 8(a) compares the starting current between hard-starting (HS, $D = 1/2$ directly) and soft-starting control algorithms (SS, D increases from 0 to 1/2 slowly and smoothly). Fig. 8(b) shows the output voltage for these two starting algorithms. In order to decrease the current impact, phase shift D should be tuned smoothly during the starting process.

However, if the initial voltage $V_2 = 0$ V, the currents of hard-starting and soft-starting control are very similar, as shown in Fig. 8(c) and (d). At this circumstance, the starting current is not determined by the control algorithm, but by the peripheral circuit. Since the transformer secondary voltage is zero, the largest current appears in the first half period

$$i_{\max} = \frac{V}{L_S}\Delta t = \frac{V_1}{L_S}\frac{1}{2f_S}. \tag{11}$$

The maximum current in (11) has no connection with phase shift D when $V_2 = 0$. It is only a function of V_1, L_s, and f_s. Therefore, the soft-starting control algorithm is revoked, as in any optimal control [16].

For a traditional SPS-based DAB dc–dc converter, one of the most important design issues is the leakage inductance L_s, which is a tradeoff between current impact and maximum output power in the steady state. For the insulated gate bipolar transistors (IGBTs) with current thresholds 65 A shown in Fig. 9, the inductance selection must fall in range A for 10 kHz switching frequency. Failure to design L_s within A will cause either overcurrent or insufficient output power. However, when the inrush current during the starting process is considered, the needed leakage inductance falls into a different region, as shown in Fig. 9. There is no intersection for the inductance selection to both restrain starting inrush current at $V_2 = 0$ and provide the rated output power simultaneously. Hence, in high-voltage and high-power applications, the starting strategy with rated input voltage and zero initial output voltage is not feasible.

The remedies for limiting the inrush current are: 1) increase input voltage V_1 from zero to the rated value with a tunable transformer or a controllable rectifier; 2) precharge the output voltage V_2 and implement the soft-starting control algorithm in Fig. 8(b); and 3) use IGBT with higher current ratings. All the aforementioned methods will increase the cost and lack feasibility in real applications.

VII. DPS Control in the Starting Process of DAB DC–DC Converters

DPS control can be used to solve the inrush current problem of DAB converters. From (11), the maximum current is directly proportional to the equivalent V_1. That means that in the starting process, if μ in Fig. 5(a) is increased smoothly and slowly from zero or a relatively small value, the inrush current can be decreased significantly.

Fig. 10(a) shows the difference of transformer voltage between the SPS and DPS controls during the starting process. The inrush current impact of DPS control is suppressed significantly, as shown in Fig. 10(b), whose peak is approximately one-fourth of that of the traditional SPS control.

VIII. Other Discussions

A. Soft-Switching Range of DPS Control

The soft switching of the proposed DPS control can be analyzed according to Fig. 3(a).

1) $t = t_0$: Q_1 turns on and Q_2 turns off. Q_2 is hard switched OFF while Q_1 is switched on at zero current (ZCS ON) since current flows through the antiparalleled diode, not in Q_1.

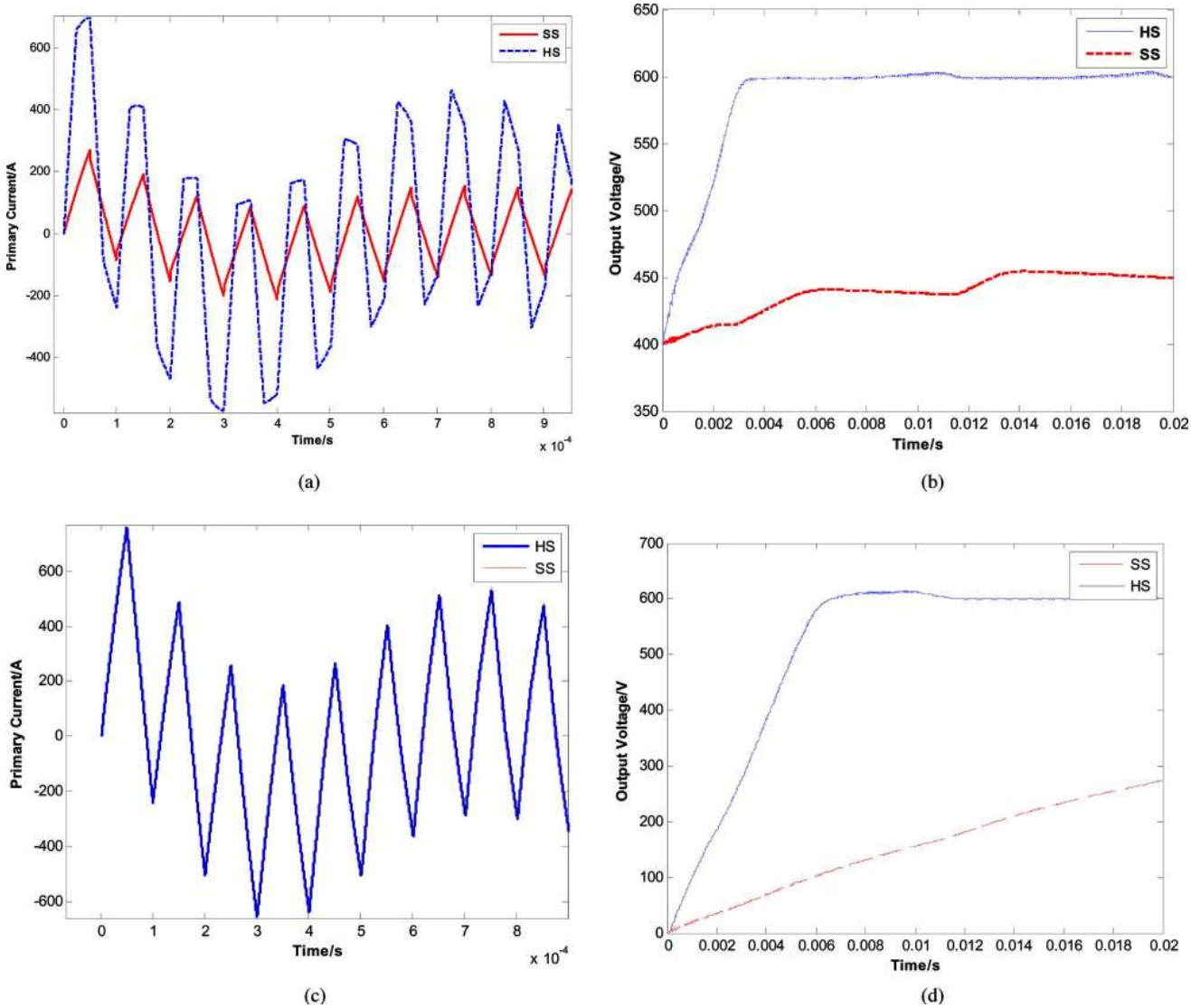

Fig. 8. SPS-based starting algorithms. (a) Current for SPS-based HS and SS ($V_2 = 400\,\mathrm{V}$). (b) Output voltage for SPS-based HS and SS ($V_2 = 400\,\mathrm{V}$). (c) Current for SPS-based HS and SS ($V_2 = 0\,\mathrm{V}$). (d) Output voltage for SPS-based HS and SS ($V_2 = 0\,\mathrm{V}$).

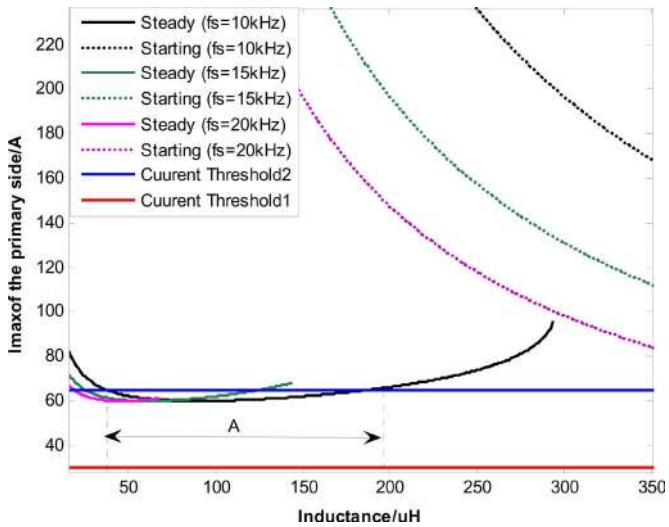

Fig. 9. Inductance selection for starting and steady operations.

2) $t = t_1$: Q_8 turns on and Q_7 turns off. Q_7 is hard switched OFF while Q_8 is ZCS ON.
3) $t = t_2$; Q_5 turns on and Q_6 turns off. Q_6 is hard switched OFF while Q_5 is ZCS ON.
4) $t = t_3$: Q_3 turns on and Q_4 turns off. Q_4 is hard switched OFF while Q_3 is ZCS ON.
5) $t = t_4$: Q_2 turns on and Q_1 turns off. Q_1 is hard switched OFF while Q_2 is ZCS ON.
6) $t = t_5$: Q_7 turns on and Q_8 turns off. Q_8 is hard switched OFF while Q_7 is ZCS ON.
7) $t = t_6$: Q_6 turns on and Q_5 turns off. Q_5 is hard switched OFF while Q_6 is ZCS ON.
8) $t = t_7$: Q_4 turns on and Q_3 turns off. Q_3 is hard switched OFF while Q_4 is ZCS ON.

Therefore, all the turn-off actions are hard-switching, while all the turn-on actions are ZCS. In the turn-on process, all the loss is in the antiparalleled diode since there is no current in the main switches. This analysis is only for Fig. 3(a) where $D_1 < D_2 <$

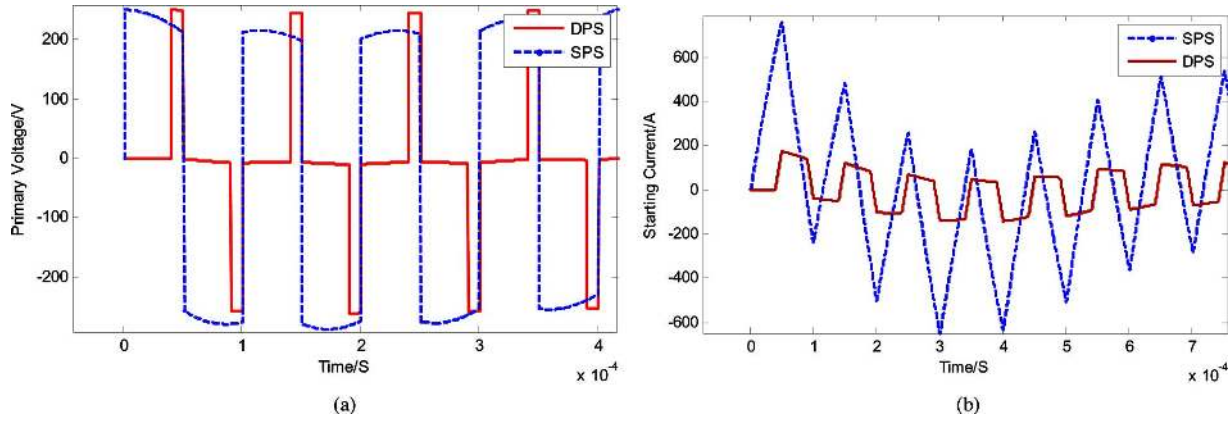

Fig. 10. Soft-starting processes under SPS and DPS control. (a) Comparison of primary voltages under SPS and DPS. (b) Comparison of currents under SPS and DPS.

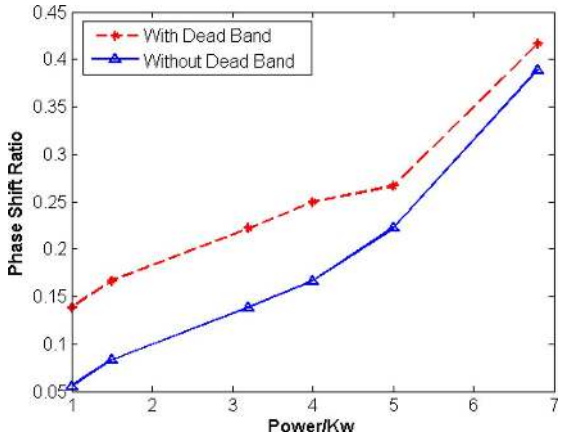

Fig. 11. Comparison of phase-shift angle in the steady state to maintain constant output voltage in SPS control.

$1 - D_1$. For other operation modes, such as $1 - D_1 < D_2 < 1$, the current waveform is different; therefore, the soft-switching range will also be different.

B. *Influence of Deadband on SPS and DPS*

DPS control is very effective for operation conditions when the output power is below the rated power. However, at these operation conditions, the deadband effect becomes significant. With the increase of the deadband time, the performance of any control algorithm will deteriorate. For example, for traditional SPS control, the phase-shift angle distorted by the deadband needs to be compensated in order to maintain the desired output power. Fig. 11 shows the needed phase-shift angle affected by the deadband. It can be seen that under light-load conditions, the deadband effect is much more severe than that under heavy-load conditions. Fig. 12 illustrates the influences of a deadband on the phase shift. Q_1–Q_8 are the gate signals for the corresponding IGBTs for SPS and DPS control, respectively.

The shadow area is the deadband, which pushes the rising edges of gate signals backward accordingly. For SPS, all the IGBTs in the same H-bridge modules are turned off during the deadband, where the output voltage is determined by the current direction. When $I(t_0) < 0$ (inside the bridge) the output voltages are nearly the same with the no-deadband ideal operation. When $I(t_0) > 0$, a phase shift $\Phi_{\rm db}$ is erased from the output voltage due to the uncontrolled state. Whether for SPS or DPS, when $I(t_0) > 0$, in order to maintain the output voltage to be the same as that in the ideal operation, an additional phase-shift angle

$$\phi_{db} = T_{\rm deadband}{}^{*}2\pi f_S \tag{12}$$

is needed to compensate the phase shift ϕ^* derived from the ideal operation. With the increase of the deadband time, the inherent ϕ_{db} will occupy a larger portion

$$\phi = \phi^* + \phi_{db} \tag{13}$$

where ϕ^* is the ideal shift angle calculated by (1). This deadband compensation shift ϕ_{db} will limit the advantage of any advanced control strategy, especially in high-voltage and high-power converters, where the deadband designed is large to guarantee the reliability of the safe operation of semiconductor switches. For DPS control, the deadband will not influence D but will erase μ, the pulsewidth of the primary and secondary voltages. In Fig. 12(c), V_p' and V_s' are the voltage waveforms affected by the deadband. Since within the deadband, the system is in the uncontrolled state, deadband generally deteriorates the performance of the system, as shown in Fig. 13.

Whether for SPS or DPS control, the deadband effect is compensated for by the PI modulators automatically. However, for SPS control, such a deadband effect is hard to compensate due to the abrupt variation of the current direction during the deadband, especially when the load changes. This is very different from inverter design where the deadband can be compensated easily [17], since the duty ratio of gate signals is varied during each fundamental period.

For DPS control, assume that $nV_1 > V_2$, then $I(t_0) < 0$, where no deadband compensation is needed. When $nV_1 < V_2$, $I(t_0) > 0$, where the deadband effect emerges. However, during the deadband, the current direction will be maintained as positive regardless of the load condition. Thus, it is very easy to implement deadband compensation without any current sensor, which is very important for future digital system design.

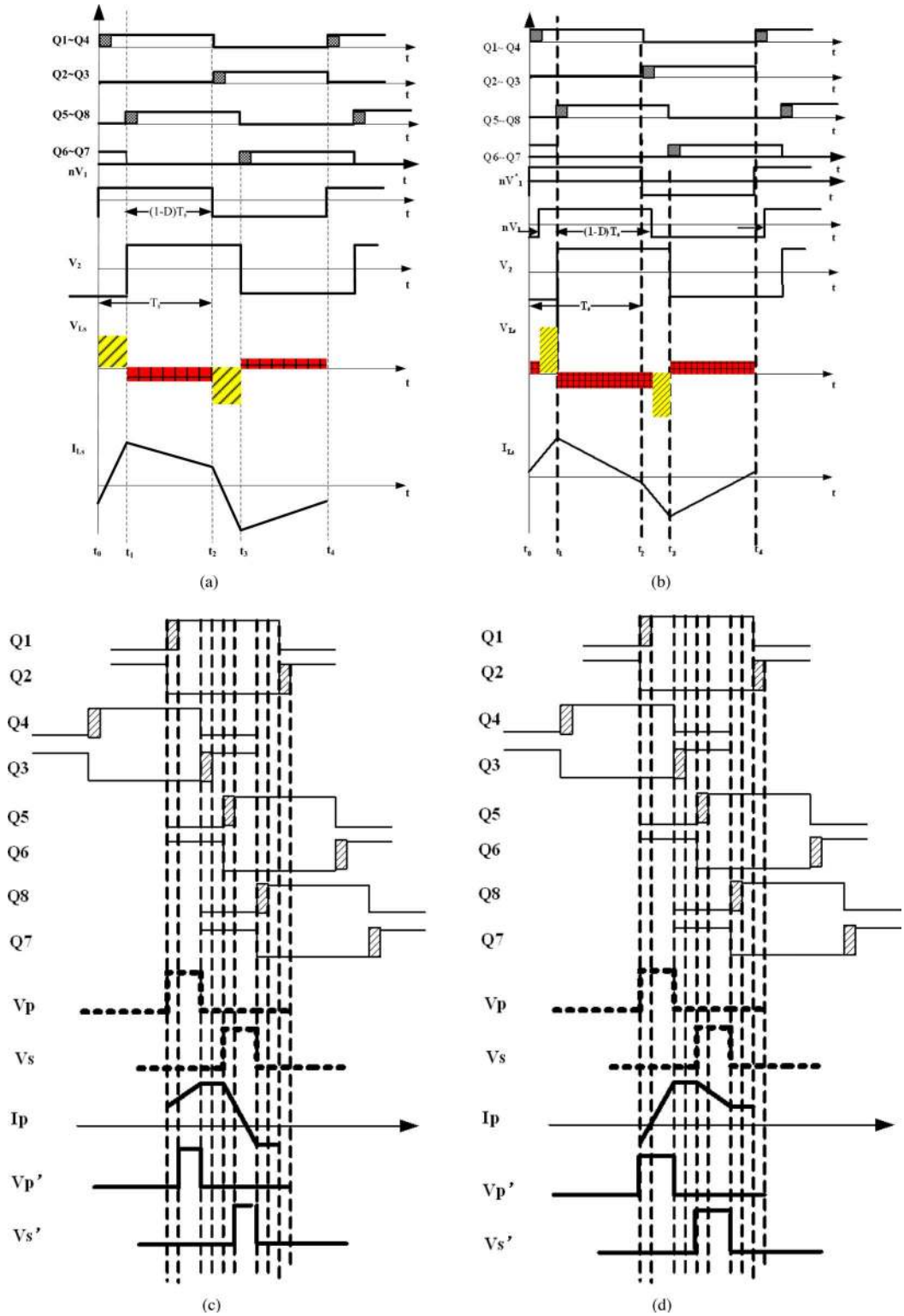

Fig. 12. Influence of the deadband on the phase shift. (a) Heavy load ($I(t_0) < 0$), for SPS. (b) Light load ($I(t_0) > 0$), for SPS. (c) $nV_1 < V_2$ ($I(t_0) > 0$), for DPS. (d) $nV_1 > V_2$ ($I(t_0) < 0$), for DPS.

It can be seen from Fig. 13 that when deadband increases, both static error and dynamic response time of the output voltage are deteriorated. More generally, it could be predicted that other short-time-scale factors, such as nonlinearity of semiconductor switches, stray parameters, and implementation time of microcontrollers, are key factors affecting the performance of the control algorithms. This is one of the reasons why most advanced control algorithms are not yet practicable in real applications.

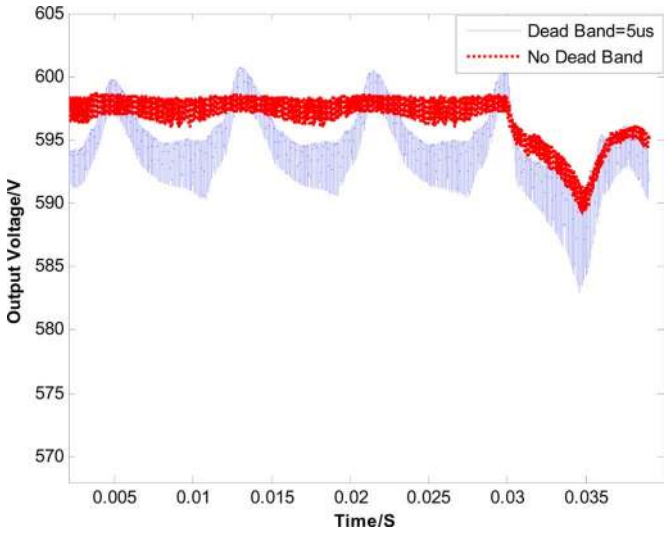

Fig. 13. Deadband influence on DPS control.

IX. Conclusion

In order to overcome the inherent disadvantages of traditional SPS control, this paper proposed a novel DPS control, which adjusts the duty ratio of the primary and secondary voltages of the high-frequency isolation transformer between 0% and 50%, and simultaneously shifts the gate signals between the primary and secondary voltages. The DPS control is essentially a variable pulsewidth plus phase-shift control. Simulation shows that DPS control not only offers excellent steady-state and dynamic performance but also improves the system efficiency. It can also be used in the starting process to limit high inrush current without the need for additional hardware. The deadband effect is also easier to compensate in DPS control than in SPS control.

Our first-stage work still lacks the detailed experiments. The work in [18] is similar to our work, although only modulating the duty ratio of the primary-side voltage, where the efficiency is higher than traditional SPS. Further effort is needed to validate the earlier theoretical analysis.

References

[1] H. J. Chiu and L. W. Lin, "A bidirectional DC–DC converter for fuel cell electric vehicle driving system," *IEEE Trans. Power Electron.*, vol. 21, no. 4, pp. 950–958, Jul. 2006.

[2] S. Y. Lee, A. G. Pfaelzer, and J. D. van Wyk, "Comparison of different designs of a 42-V/14-V DC/DC converter regarding losses and thermal aspects," *IEEE Trans. Ind. Appl.*, vol. 43, no. 2, pp. 520–530, Mar./Apr. 2007.

[3] K. H. Cheng, C. F. Hsu, C. M. Lin, T. T. Lee, and C. Li, "Fuzzy–neural sliding-mode control for DC–DC converters using asymmetric gaussian membership functions," *IEEE Trans. Ind. Electron.*, vol. 54, no. 3, pp. 1528–1536, Jun. 2007.

[4] S. C. Tan, Y. M. Lai, and C. K. Tse, "A unified approach to the design of PWM-based sliding-mode voltage controllers for basic DC–DC converters in continuous conduction mode," *IEEE Trans. Circuits Syst. I, Reg. Papers*, vol. 53, no. 8, pp. 1816–1827, Aug. 2006.

[5] T. S. Chong, Y. M. Lai, and C. K. Tse, "An evaluation of the practicality of sliding mode controllers in DC–DC converters and their general design issues," in *Proc. IEEE Power Electron. Spec. Conf. (PESC 2006)*, Jeju, South Korea, pp. 1–7.

[6] C. H. Rivetta, A. Emadi, G. A. Williamson, R. Jayabalan, and B. Fahimi, "Analysis and control of a buck DC–DC converter operating with constant power load in sea and undersea vehicles," *IEEE Trans. Ind. Appl.*, vol. 42, no. 2, pp. 559–572, Mar./Apr. 2006.

[7] J. L. D. Gomez, E. G. Cervantes, D. R. L. Flores, P. N. Enjeti, and L. Palma, "Analysis and evaluation of a series-combined connected boost and buck-boost dc–dc converter for photovoltaic application," in *Proc. Appl. Power Electron. Conf. (APEC 2006)*, pp. 979–987.

[8] M. N. Kheraluwala, R. W. Gascoigne, D. M. Divan, and E. D. Baumann, "Performance characterization of a high-power dual active bridge DC-to-DC converter," *IEEE Trans. Ind. Appl.*, vol. 28, no. 6, pp. 1294–1301, Nov./Dec. 1992.

[9] R. W. DeDoncker, M. H. Kheraluwala, and D. M. Divan, "Power conversion apparatus for DC/DC conversion using dual active bridges," U.S. Patent 5027264, Jun. 25, 1991.

[10] D. H. Xu, C. H. Zhao, and H. F. Fan, "A PWM plus phase-shift control bidirectional DC–DC converter," *IEEE Trans. Power Electron.*, vol. 19, no. 3, pp. 666–675, May 2004.

[11] L. Zhu, "A novel soft-commutating isolated boost full-bridge ZVS–PWM DC–DC converter for bidirectional high power applications," *IEEE Trans. Power Electron.*, vol. 21, no. 2, pp. 422–429, Mar. 2006.

[12] Z. L. Zhang and X. B. Ruan, "A novel double phase-shift control scheme for full-bridge three-level converter," in *Proc. Appl. Power Electron. Conf. (APEC 2005)*, vol. 2, pp. 1240–1245.

[13] L. Zhu, J. S. Lai, and F. C. Lee, "Start-up circuit and control for high power isolated DC/DC converters," U.S. Patent US 6587356 B2, Jul. 1, 2003.

[14] F. Z. Peng, L. Hui, S. G. Jia, and J. S. Lawler, "A new ZVS bidirectional DC–DC converter for fuel cell and battery application," *IEEE Trans. Power Electron.*, vol. 19, no. 1, pp. 54–65, Jan. 2004.

[15] Z. Ye, P. Jain, and P. Sen, "Circulating current minimization in high frequency AC power distribution architectures with multiple inverter modules operated in parallel," *IEEE Trans. Ind. Electron.*, vol. 54, no. 5, pp. 2673–2687, Oct. 2007.

[16] Z. M. Zhao, H. Bai, and L. Q. Yuan, "Transient of power pulse and its sequence in power electronics," *Sci. China, Series E: Technol. Sci.*, vol. 50, no. 3, pp. 351–360, Jun. 2007.

[17] N. Urasaki, T. Senjyu, K. Uezato, and T. Funabashi, "Adaptive dead-time compensation strategy for permanent magnet synchronous motor drive," *IEEE Trans. Energy Convers.*, vol. 22, no. 2, pp. 271–280, Jun. 2007.

[18] G. G. Oggier, R. Leidhold, G. O. Garcia, A. R. Oliva, J. C. Balda, and F. Barlow, "Extending the ZVS operating range of dual active bridge high-power DC–DC converters," in *Proc. IEEE Power Electron. Spec. Conf. (PESC 2006)*, Jeju, South Korea, pp. 1–7.

Hua Bai received the B.S. and Ph.D. degrees from the Department of Electrical Engineering, Tsinghua University, Beijing, China, in 2002 and 2007, respectively.

He is currently a Post-doctoral Fellow at the University of Michigan, Dearborn. His current research interests include the dynamic processes and transient pulse power phenomena of power electronic devices, especially in a three-level neutral point clamped (NPC) high-voltage high-power inverter and an isolated bidirectional dc–dc converter.

Chris Mi (S'00–A'01–M'01–SM'03) received the B.S. and M.S. degrees from Northwestern Polytechnical University, Xi'an, China, in 1985 and 1988, respectively, and the Ph.D. degree from the University of Toronto, Toronto, ON, Canada, in 2001, all in electrical engineering.

He is currently an Associate Professor at the University of Michigan, Dearborn. From 2000 to 2001, he was with General Electric Company.

Prof. Mi received the "National Innovation Award" and the "Government Special Allowance," and was the recipient of the 2005 "Distinguished Teaching Award" of the University of Michigan, where he is also the Chair of the IEEE Southeast Michigan Section. He was also a recipient of the 2007 IEEE Region 4 "Outstanding Engineer Award," and the 2007 IEEE Southeastern Michigan Section "Outstanding Professional Award." He recently won the 2007 SAE Environmental Excellence in Transportation (E2T) Award.